Atmospheric, Evolutionary, and Spectral Models of the Brown Dwarf Gliese 229 B

M. S. Marley,* D. Saumon, T. Guillot, R. S. Freedman, W. B. Hubbard, A. Burrows, J. I. Lunine

Theoretical spectra and evolutionary models that span the giant planet–brown dwarf continuum have been computed based on the recent discovery of the brown dwarf Gliese 229 B. A flux enhancement in the 4- to 5-micrometer wavelength window is a universal feature from jovian planets to brown dwarfs. Model results confirm the existence of methane and water in the spectrum of Gliese 229 B and indicate that its mass is 30 to 55 jovian masses. Although these calculations focus on Gliese 229 B, they are also meant to guide future searches for extrasolar giant planets and brown dwarfs.

Brown dwarfs inhabit a realm intermediate between the more massive stars and the less massive planets. Their thermal infrared emission is powered by the release of gravitational potential energy as regulated by their atmospheres. Long known only as theoretical constructs, the discovery of the first unimpeachable brown dwarf (*1*, *2*) allows a detailed study of a representative of this population of objects. Gliese (Gl) 229 B, the recently discovered companion to Gl 229 A, has an estimated luminosity L of $6.4 \pm 0.6 \times 10^{-6}$ $L_\odot$ ($L_\odot$ is the solar luminosity), an effective temperature T_{eff} below 1200 K, and a clear signature of methane (CH_4) in its spectrum (*3*). Because there can be no stars cooler than 1700 K with luminosities below 5×10^{-5} $L_\odot$ or with CH_4 bands (*4*), the status of Gl 229 B as one of the long-sought brown dwarfs is now beyond question. However, models of its atmosphere and evolution are required if its physical properties are to be derived. The previous lack of observations has inhibited the generation of theoretical spectra. To remedy this, we coupled model spectra and evolutionary calculations to estimate the object's T_{eff}, L, surface gravity g, mass M, radius R, and age t and to find useful spectral diagnostics. The recent discoveries of planets 51 Pegasi B, 70 Virginis B, 47 Ursae Majoris B, and Gl 411 B (*5*) have doubled the number of known jovian planets. There is now an extraordinarily rich variety of low-temperature, low-mass [0.3 to 84 M_J (M_J is the mass of Jupiter)] planets and brown dwarfs. Our improved evolutionary models and spectra, here applied to Gl 229 B, are meant to facilitate the study and interpretation of these objects.

To compute the atmospheric temperature profile for brown dwarfs in the relevant temperature range (600 to 1200 K), we adapted a model that was originally constructed to study the atmospheres of the jovian planets and Titan (*6*). We assumed a standard solar composition for the bulk of the atmosphere (*7*). Refractory elements (for example, Fe, Ti, and silicates) condense deep in the atmosphere for $T_{eff} \approx 1000$ K and thus have negligible gas-phase abundances near the photosphere, as is also true in the atmosphere of Jupiter (T_{eff} = 124 K). For an atmosphere similar to that of Gl 229 B, chemical equilibrium calculations indicate that C, N, O, S, and P will be found mainly in the form of CH_4, ammonia (NH_3), water (H_2O), hydrogen sulfide (H_2S), and phosphine (PH_3), respectively. However, deep in the atmosphere, chemical equilibrium favors

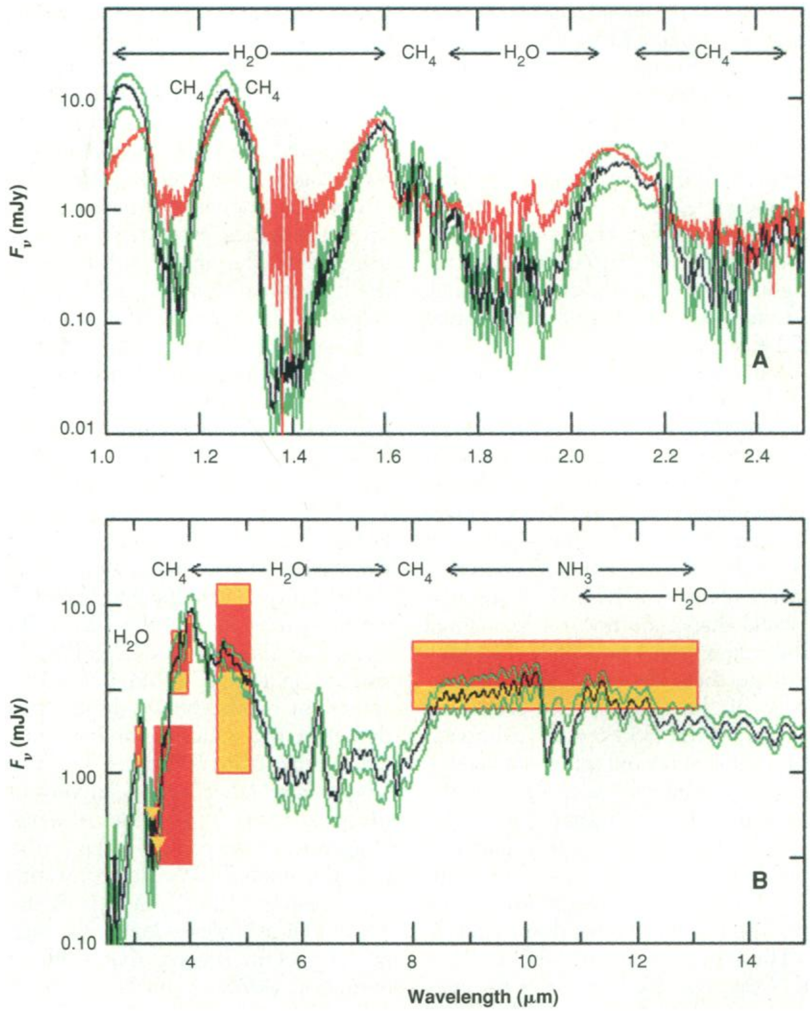

Fig. 1. **(A)** Synthetic spectra for (bottom to top) T_{eff} = 890 K (green), 960 K (black), 1030 K (green) and g = 1000 m s^{-2}, together with data (*3*) (red line). The three curves in **(B)** are calculated for the same values of T_{eff} and g; colored boxes show the photometric measurements with bandpasses indicated by their width. The red region shows the 1σ error on the measurements and yellow gives the 2σ error. Yellow triangles show upper limits to narrow-band fluxes. In both (A) and (B), spectral intervals are labeled with the molecules primarily responsible for the opacity in that interval. Flux F_ν is in millijanskys (1 mJy = 10^{-29} W m^{-2} Hz^{-1}).

M. S. Marley, Department of Astronomy, New Mexico State University, Box 30001, Department 4500, Las Cruces, NM 88003, USA.
D. Saumon, T. Guillot, W. B. Hubbard, J. I. Lunine, Lunar and Planetary Laboratory, University of Arizona, Tucson, AZ 85721, USA.
R. S. Freedman, Sterling Software, NASA Ames Research Center, Moffett Field, CA 94035, USA.
A. Burrows, Departments of Physics and Astronomy, University of Arizona, Tucson, AZ 85721, USA.
*To whom correspondence should be addressed. E-mail: mmarley@nmsu.edu

carbon monoxide (CO) over CH_4 and molecular nitrogen (N_2) over NH_3. Our model atmosphere incorporates opacities of these molecules, molecular hydrogen (H_2), and He (*8*) in their respective solar abundances and includes no other elements.

To constrain the properties of Gl 229 B, we constructed a grid of brown dwarf model atmospheres with T_{eff} ranging from 600 to 1200 K and $100 < g < 3200$ m s^{-2}. For each case, we computed a self-consistent radiative-convective equilibrium temperature profile and the emergent radiative flux (*9*). Absorption of radiation from Gl 229 A is included in our model but contributes negligibly to Gl 229 B's energy balance, owing to the large orbital separation ($\geq$44 astronomical units) and faintness of Gl 229 A.

Emergent spectra of brown dwarf atmosphere models compared to observed fluxes (Fig. 1, A and B) (*1*, *10*) show the influence of a minimum in the molecular opacities at wavelengths λ around 4 to 5 μm. As in the case of Jupiter, this minimum allows radiation to escape from deep warm regions of the atmosphere. Clearly, this wavelength region is favorable for brown dwarf searchers in the future. By comparison, the widely used K band at 2.2 μm is greatly suppressed by strong CH_4 and H_2–H_2 absorption features. Beyond 13 μm, the decreasing flux falls slightly more rapidly than a Planck distribution with a brightness temperature near 600 K.

Our computed spectra (Fig. 1) are a good match with the data in the 1.2- to 1.8-μm window, but they deviate at 1 μm, in the window centered on 2.1 μm, and in regions of low flux. Our best fitting models reproduce the observed broadband fluxes (*3*) reasonably well. Although many individual spectral features of CH_4 and H_2O are reproduced, particularly near 1.7 and 2.0 μm, the overall band shapes are not well accounted for in the region from 1 to 2.5 μm (Fig. 1A). We attribute these discrepancies to a poor knowledge of the CH_4 opacity and, to a lesser extent, of the H_2O opacity. Although we have combined several sources of varying accuracy (*8*) to generate as complete a description of the CH_4 opacity as possible, CH_4 line lists are based on laboratory measurements at room temperature and do not include lines from higher energy levels that would be populated at brown dwarf temperatures. Thus, the opacity of CH_4 at $T \approx$ 1000 K is the most likely cause of the mismatches seen in the 1.6- to 1.8-μm band and at $\lambda > 2.1$ μm.

Clouds may alter the atmospheric structure and spectrum of Gl 229 B, as they do in the atmospheres of planets in our solar system. Extrapolating from results for Jupiter (*11*) and using more recent chemical equilibrium calculations (*12*), we find that the following additional molecules are expected to condense between 10^{-3} and 10 bar: $NH_4H_2PO_4$, ZnS, K_2S, Na_2S, and MnS. If a relatively large proportion of condensed particles is retained in the atmosphere, cloud layers could affect the structure of the brown dwarf, making it hotter by as much as 100 K at 1 bar (depending on the uncertain particle sizes and optical properties). Clouds might increase the flux in the K band, because of the higher temperatures, and lower the flux below 1.3 μm, as a result of scattering.

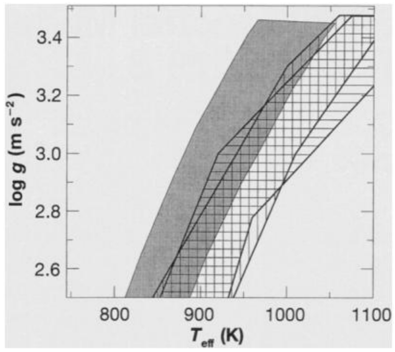

Fig. 2. Limits on T_{eff} and g for Gl 229 B. The shaded area delimits the effective temperature and gravity of model objects that match within 2σ the observed bolometric luminosity (3) of Gl 229 B at any age. The other areas show limits from fitting the 1- to 2.5-μm spectrum (vertical lines) and the 2.5- to 13-μm photometry (horizontal lines).

Given these uncertainties, our best fits for the bolometric luminosity, the observed spectrum, and the photometry give combinations of T_{eff} and g lying in the range 850 K $< T_{eff} <$ 1100 K and $g < 3000$ m s^{-2} (Fig. 2). Lower T_{eff} values are allowed for $g < 300$ m s^{-2}, but the shapes of the J and H bands increasingly deviate from the observations. The high-T_{eff} limit arises from the inability to simultaneously fit the bolometric luminosity and the 10-μm flux.

A determination of Gl 229 B's gravity by spectral matching would impose a direct constraint on the brown dwarf's mass. Although g is a function of both mass and radius, the radii of brown dwarfs in this temperature range vary relatively little as the mass varies by an order of magnitude. However, at the present stage of the analysis, the gravity is poorly constrained because high g–high T_{eff} models fit the spectra as well as lower g–lower T_{eff} ones. The model spectra suggest that high spectral resolution ($\lambda/\Delta\lambda \gtrsim 1000$) observations at 1.8 to 2.1 μm may provide a tighter constraint on g.

The depth at which the atmosphere becomes convective depends on the specified model gravity and T_{eff}. At the highest pressure point of each model atmosphere, where the temperature-pressure profile merges

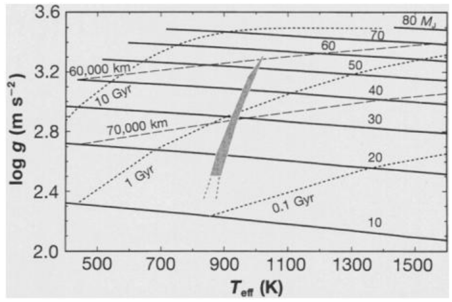

Fig. 3. The shaded area shows the region of overlap of the three constraints from Fig. 2 (the cutoff at low g is arbitrary). Solid lines depict the evolution of T_{eff} and g as brown dwarfs of various mass cool. Several contours of constant radius (dashed curves) and constant age (dotted curves) are also shown. Gyr, 10^9 years; M_J, Jupiter mass.

with an adiabat, the interior entropy is calculated for the purpose of matching an interior temperature distribution to the given values of (T_{eff},g). The full evolutionary behavior of a brown dwarf can be obtained by supplementing previous boundary conditions for objects with masses ~0.3 to 15 M_J (*13*, *14*) with our grid of nongray model atmospheres. Such evolutionary models are needed because R varies with mass and age by up to 30%. The precise R of the object is important because we must match not only Gl 229 B's spectrum but also the inferred bolometric luminosity: $L = 4\pi R^2 \sigma T_{eff}^4$ (σ is the Stefan-Boltzmann constant). Our results can be summarized by the following approximate fitting formulas (g is in meters per second squared, T_{eff} is in kelvin):

$$M = 36M_J \left(\frac{g}{1000}\right)^{0.64} \left(\frac{T_{eff}}{1000}\right)^{0.23} \quad (1)$$

$$t = 1.1 \times 10^9 \text{years} \left(\frac{g}{1000}\right)^{1.7} \left(\frac{T_{eff}}{1000}\right)^{-2.8} \quad (2)$$

$$R = 67200 \text{ km} \left(\frac{g}{1000}\right)^{-0.18} \left(\frac{T_{eff}}{1000}\right)^{0.11} \quad (3)$$

The effective temperature and surface gravity of Gl 229 B can now be constrained by three sets of observations (which are not independent of each other): (i) the observed spectrum from 1 to 2.5 μm, (ii) the broadband flux in several bandpasses from 2 to 13 μm (*10*), and (iii) the bolometric luminosity of the object (*3*). These constraints then limit $g < 2200$ m s^{-2} and T_{eff} = 960 $\pm$ 70 K (Fig. 2). Because the reported age of Gl 229 A is $\gtrsim 1 \times 10^9$ years (*1*), g is further constrained to lie in the range 800 to 2200 m s^{-2} (Fig. 3).

In the atmospheres of Gl 229 B and Jupiter, convection commences as the optical depth to thermal photons becomes large, and

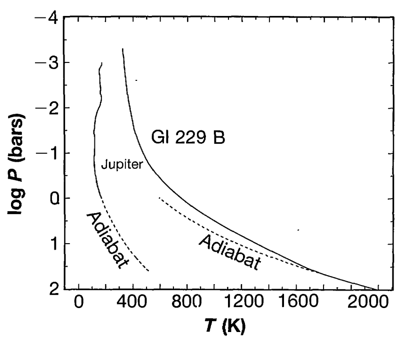

Fig. 4. Calculated atmospheric structure for Gl 229 B (solid curve); the dashed curve shows an adiabat corresponding to the deep interior temperature profile. For comparison, an observed profile for Jupiter (*16*) is shown (solid), along with its calculated prolongation into the adiabatic deep interior (dashed curve).

the temperature profile closely approaches an adiabatic profile at deeper levels because of efficient convection (Fig. 4). In some models, particularly the lower gravity models and those with $T_{eff} < 900$ K, the radiative-equilibrium lapse rate exceeds the adiabatic lapse rate over a several-bar region near $P = 1$ bar. These atmospheres exhibit two convective regions, a lower region presumably continuing to great depth and an upper, detached convective zone. Such a detached convective zone is also predicted for the atmosphere of Jupiter (*15*).

Our estimate of T_{eff} of 960 ± 70 K and a gravity between 800 and 2200 m s^{-2} for the brown dwarf Gl 229 B translates into masses and ages of 30 to 55 M_J and 1×10^9 to 5×10^9 years, respectively. As Eq. 1 and Fig. 3 indicate, gravity maps almost directly into mass, and ambiguity in the former results in uncertainty in the latter. Because the inferred mass of Gl 229 B exceeds that required for deuterium burning (*14*), deuterium-bearing molecules should not be present in its atmosphere. Although the near-infrared spectrum of Gl 229 B is dominated by H_2O, we confirmed the presence of CH_4 in the atmosphere from our modeling of its features at 1.6 to 1.8 μm, 2.2 to 2.4 μm, and 3.2 to 3.6 μm. In addition, we found a flux enhancement in the window at 4 to 5 μm throughout the T_{eff} range from 124 K (Jupiter) through 1300 K, and hence we believe that this band is a universal diagnostic for brown dwarfs and jovian planets.

REFERENCES AND NOTES

1. T. Nakajima *et al.*, *Nature* **378**, 463 (1995).
2. B. R. Oppenheimer, S. R. Kulkarni, K. Matthews, T. Nakajima, *Science* **270**, 1478 (1995).
3. K. Matthews, T. Nakajima, S. R. Kulkarni, B. R. Oppenheimer, in preparation; T. R. Geballe, S. R. Kulkarni, C. E. Woodward, G. C. Sloan, *Astrophys. J.*, in press.
4. A. Burrows, W. B. Hubbard, D. Saumon, J. I. Lunine, *Astrophys. J.* **406**, 158 (1993); J. I. Lunine, W. B. Hubbard, M. S. Marley, *ibid.* **310**, 238 (1986).
5. M. Mayor and D. Queloz, *Nature*, **378**, 355 (1995); G. W. Marcy and R. P. Butler, *Astrophys. J.*, in press; R. P. Butler and G. W. Marcy, *ibid.*, in press; G. Gatewood, *Bull. Am. Astron. Soc.* **28**, 885 (1996).
6. C. P. McKay, J. B. Pollack, R. Courtin, *Icarus* **80**, 23 (1989); M. S. Marley, C. P. McKay, J. B. Pollack, in preparation.
7. E. Anders and N. Grevesse, *Geochim. Cosmochim. Acta* **53**, 197 (1989).
8. The opacity calculations include collision-induced absorption by H_2–H_2 [A. Borysow and L. Frommhold, *Astrophys. J.* **348**, L41 (1990)] and H_2–He [C. Zheng and A. Borysow, *Icarus* **113**, 84 (1995), and references therein], free-free absorption by H_2^- [K. L. Bell, *J. Phys. B* **13**, 1859 (1980)], bound-free absorption by H^- [T. L. John, *Astron. Astrophys.* **193**, 189 (1988)], and Rayleigh scattering. We calculated the absorptions of NH_3, CH_4, and PH_3 using the HITRAN database [J. C. Hilico, M. Loete, L. R. Brown Jr., *J. Mol. Spectrosc.* **152**, 229 (1992)] with corrections and extensions. Additional tabulations [K. Strong, F. W. Taylor, S. B. Calcutt, J. J. Remedios, J. Ballard, *J. Quant. Spectrosc. Radiat. Transfer* **50**, 363 (1993)] were used where necessary for CH_4, especially shortward of 1.6 μm. Data for H_2O and H_2S were computed from a direct numerical diagonalization [R. B. Wattson and L. S. Rothman, *ibid.* **48**, 763 (1992)] by R. B. Wattson (personal communication). Absorption by CO [J. B. Pollack *et al.*, *Icarus* **103**, 1 (1993)] and PH_3 was included in the spectral models but not in the temperature profile computation. The baseline models assume that the atmosphere is free of clouds.
9. For the temperature profile computation, we treated the molecular opacity using the *k*-coefficient method [R. Goody, R. West, L. Chen, D. Crisp, *J. Quant. Spectrosc. Radiat. Transfer* **42**, 539 (1989)]. After a radiative-equilibrium temperature profile was found, we iteratively adjusted the atmosphere to self-consistently solve for the size of the convection zones, given the specified internal heat flux. Given the radiative-convective temperature-pressure profiles, we generated high-resolution synthetic spectra by solving the radiative transfer equation [P. Bergeron, F. Wesemael, G. Fontaine, *Astrophys. J.* **367**, 253 (1991)]. Eighteen thousand frequency points were used in the spectral region from 1 to 15.4 μm. These spectra were smoothed with a Gaussian-bandpass filter giving a final resolution of $\lambda/\Delta\lambda = 600$.
10. K. Matthews, T. Nakajima, S. Kulkarni, B. Oppenheimer, *Int. Astron. Union Circ. 6280* (1995).
11. B. Fegley Jr. and K. Lodders, *Icarus* **110**, 117 (1994).
12. K. Lodders, personal communication.
13. A. Burrows, D. Saumon, T. Guillot, W. B. Hubbard, J. I. Lunine, *Nature* **375**, 299 (1995).
14. D. Saumon *et al.*, *Astrophys. J.* **460**, 993 (1996).
15. T. Guillot, D. Gautier, G. Chabrier, B. Mosser, *Icarus* **112**, 337 (1994).
16. G. Lindal, *Astron. J.* **103**, 967 (1992).

17. D.S. is a Hubble Fellow. T.G. is supported by the European Space Agency. This research was supported by grants from NASA and NSF. We thank T. Geballe for digital versions of the Gl 229 B spectrum, K. Lodders for chemical-equilibrium calculations, and K. Zahnle for an insightful review.

21 March 1996; accepted 5 June 1996

Off-Resonance Conduction Through Atomic Wires

Ali Yazdani, D. M. Eigler, N. D. Lang

The electrical resistance of wires consisting of either a single xenon atom or two xenon atoms in series was measured and calculated on the basis of an atom-jellium model. Both the measurement and the calculation yielded a resistance of 10^5 ohms for the single–xenon atom system and 10^7 ohms for the two–xenon atom system. These resistances greatly exceeded the 12,900-ohm resistance of an ideal one-dimensional conduction channel because conduction through the xenon atoms occurs through the tail of the xenon 6*s* resonance, which lies far above the Fermi level. This conduction process in an atom-sized system can now be understood in terms of the electronic states of individual atoms.

Our understanding of the electron transport properties of macroscopic and mesoscopic bodies is relatively mature compared to our fledgling understanding of transport through nanometer-scale structures composed of just a few atoms. Transport through such structures is of particular interest because of its perceived importance in possible future device technologies. We address the question of how strong a role the electronic properties of a single atom play in determining the motion of electrons through a nanometer-sized object.

One might expect that the idealized view of one-dimensional (1D) transport, which predicts an electrical resistance quantized in units of $h/2e^2$ (where h is Planck's constant and e is the electron charge) of 12.9 kilohms, already captures most of the physics of electron transport down to the atomic scale (*1*). Research on mesoscopic conductors such as 2D electron gas devices realized in semiconductor heterostructures has shown the importance of such a conductance quantization in devices involving ballistic transport of electrons (*2*). However, conductance on a smaller scale, through a chain of just a few atoms, may depend on the atomic orbitals. More generally, one can ask if there are some principles by which we could understand the atomic-scale conduction process without extensive calculation in every case. We

A. Yazdani and D. M. Eigler, IBM Research Division, Almaden Research Center, 650 Harry Road, San Jose, CA 95120, USA.
N. D. Lang, IBM Research Division, Thomas J. Watson Research Center, Yorktown Heights, NY 10598, USA.